# Deep Breathing Couples CSF and Venous Fluid Dynamics

**Jost M Kollmeier**
Biomedizinische NMR, Max-Planck-Institut für biophysikalische Chemie, Göttingen
**Lukas Gürbüz-Reiss**
Department of Pediatrics and Adolescent Medicine, University Medical Center Göttingen
**Simon Badura**
Department of Pediatrics and Adolescent Medicine, University Medical Center Göttingen
**Ben Ellebracht**
Department of Pediatrics and Adolescent Medicine, University Medical Center Göttingen
**Jutta Gärtner**
Department of Pediatrics and Adolescent Medicine, University Medical Center Göttingen
**Hans-Christoph Ludwig**
Department of Neurosurgery, Division of Pediatric Neurosurgery, University Medical Center Göttingen
**Jens Frahm**
Biomedizinische NMR, Max-Planck-Institut für biophysikalische Chemie Göttingen
**Steffi Dreha-Kulaczewski** ( sdreha@gwdg.de )
University Medical Center Göttingen https://orcid.org/0000-0003-4951-3176

**Research**

**Keywords:** real-time phase-contrast flow MRI, CSF dynamics, venous flow, forced breathing, venous-CSF coupling

**Posted Date:** May 14th, 2021

**DOI:** https://doi.org/10.21203/rs.3.rs-514955/v1

# Abstract

**Background:** Deep inspiration acts as a driving force for eliciting an upward flow of CSF into the brain simultaneous to an increase of venous outflow to the heart. These findings suggest two interconnected fluid systems which together play a pivotal role in maintaining constant intracranial pressure. Moreover, venous system pathologies are increasingly connected with various disorders of CSF circulation, although exact coupling mechanisms remain unknown. The purpose of the present study was to explore the role of respiratory forces in linking both fluid systems in the upper and lower body.

**Methods:** Twelve healthy subjects (2 females, age 23-38 years) were studied using real-time phase-contrast flow MRI at 3T. Subjects followed a breathing protocol with 40 s of normal and forced respiration. CSF flow was quantified at the aqueduct and spinal levels C3 and L3. Venous flow was studied in the internal jugular veins and cervical epidural veins and in the inferior vena cava and lumbar epidural veins. Flow values (ml $s^{-1}$), ROI sizes ($mm^2$) and flow frequency components (Hz) were determined and Wilcoxon signed-rank and paired t-tests employed to calculate p values.

**Results:** Cardiac-related flow components prevailed during normal breathing. Forced respiration shifted the main frequency component for CSF and venous dynamics to 0.2 in line with the breathing protocol. Amplification of fluid flow during forced breathing reached significance at all positions except for lumbar and cervical epidural veins and the internal jugular vein which showed decreased flow rates. Veins of the superior and inferior parts of the body followed an opposite flow behavior.

**Conclusion:** Our results support the notion that deep respiration acts as a coupling mechanism of the interdependent venous and CSF flow. Surpassing a certain threshold of intrathoracic and abdominal volume and pressure, deep breathing may perturb their cardiac-dominated fluid dynamics and prompt a synchronous increase of movements. Insights into the driving forces of CSF and venous circulation extend our understanding how the cerebral venous system may be conjunct to intracranial pressure regulations. It will further facilitate our understanding of the pathophysiology of related forms of hydrocephalus.


# Background

Recent studies of cerebrospinal fluid (CSF) circulation, pathways and dynamics have rigorously challenged century-old classical views [1–5]. Still, our understanding about the disturbances of CSF circulation underlying the various forms of hydrocephalus and syringomyelia across all ages is vastly incomplete [6]. Hence, detailed insights into regulatory forces of CSF dynamics are of imminent clinical importance to better comprehend the pathogeneses and more importantly derive the most specific therapeutic strategies.

The advent of real-time phase-contrast flow magnetic resonance imaging (MRI), a technique independent of any physiological gating [7], recently revealed the influence of respiration on the CSF movement. In particular, forced inspiration has been identified as the dominant driver which prompts an upward surge

of CSF from the lumbar region along the entire spinal canal, into the cranial vault and towards the subarachnoid and brain ventricular spaces. Small cardiac-driven CSF pulsations, most prevalent in cervical regions in close proximity to the heart, were shown to be superimposed on a dominating, high-amplitude flow component triggered by forced respiration [8–10]. Furthermore, the inspiratory lowering of the intrathoracic pressure governs venous drainage out of the head/neck region as a prerequisite to ensure adequate preload of the heart. Real-time flow MRI demonstrated fluctuations of outflow in the cervical epidural veins dependent on the strength of inhalation [10]. These latest insights point to a tightly regulated equilibrium between CSF and venous systems, that might play an essential role in regulating the intracranial volume in accordance with the Monro-Kellie doctrine [11].

The notion of a dynamic interplay between CSF and venous flow is in line with an increasingly popular holistic view on brain fluids [12, 13]. Mounting clinical evidence substantiates the importance of the cerebral venous systems for maintaining intracranial pressure (ICP) and hence its role in a broad spectrum of neurological diseases like communicating hydrocephalus and myelopathy [14, 15]. A high prevalence of extra- and intracranial venous flow obstruction has been reported in patients with idiopathic intracranial hypertension (IIH) [16]. However, the physiological mechanisms, which conjunct CSF and veins, are still poorly understood.

Our study aimed (i) to test the hypothesis that respiration represents a mechanism coupling CSF and venous fluid systems and (ii) to further elucidate the interdependence and dynamics of CSF and venous flow by extending previous measurements to the lower body as well as encompassing equal periods of normal free breathing and forced respiration in the study protocol.

## Methods

# Subjects

Twelve healthy volunteers (2 females, 10 males, age range 23–38 years, 28 ± 5; mean ± SD; height 180 ± 7 cm, weight 77 ± 12 kg, BMI 23.4 ± 2.5 kg/m²) without contraindication for MRI and no known illness were enrolled. The study was approved by the institutional review board of the University Medical Center Göttingen (#18/2/14) and written informed consent was obtained from each subject prior to MRI. The study was in compliance with the Declaration of Helsinki.

# Study Design

Three cross-sections for flow MRI measurements were chosen covering intracranial and spinal CSF and the venous systems at the aqueduct (Aqd), spinal cervical level three (C3) and spinal lumbar level three (L3). Regions of interest (ROI) for the analysis of CSF dynamics were placed in the aqueduct and spinal subarachnoid spaces at C3 and L3 as outlined in Fig. 1a-e. For corresponding venous flow determinations ROIs were drawn around the internal jugular veins (IJV) (Fig. 1c) with the stronger flow signal in the neck region and around the lumbar inferior vena cava (IVC) (Fig. 1e), respectively. The venous plexus expanding in the epidural spaces inside the entire vertebral column (internal vertebral

venous plexus) commonly forms prominent orthogonal veins at C3 which resemble a rope ladder. The more prominent epidural vein (EV) was selected for the ROI analysis (Fig. 1b). The lumbar venous plexus forms a spacious mesh rendering epidural vessels less well identifiable. ROIs in that region were defined around flow signals detectable in the epidural space ventral to the CSF space (Fig. 1d).

All subjects were examined in supine position and required to follow a visually presented breathing protocol. Timing and commands for deep inspiration and expiration were explained and trained beforehand as inspiration and exhalation had to occur gradually over 2.5 s periods. Furthermore, subjects were instructed to avoid hyperventilation. The breathing protocol started with 40 s of normal free breathing followed by 8 cycles of 2.5 s forced inspiration and 2.5 s forced expiration. The protocol concluded with another 10 s period of normal breathing summing up to a total of 90 s per scan (Fig. 2, bottom line). Subjects were without any cardiac conditions, had pulse rates within normal age limits and have been monitored via a respiration belt fixed at the level of the diaphragm. Individual breathing performance and adherence to the protocol were evaluated by visual observation and measurements were repeated if deemed necessary. The flow data were acquired in the same order for all subjects and an individual study lasted about 40–50 min.

# Real-time phase-contrast flow MRI

All data sets were acquired on a 3 Tesla scanner (Magnetom Prisma Fit, Siemens Healthcare) using real-time phase-contrast flow MRI based on highly undersampled radial FLASH sequences [17, 18] with timing-optimized gradient design [19]. Quantitative velocity maps were obtained by a model-based reconstruction technique offering access to high spatiotemporal resolutions [20]. The MRI parameters were set as follows: repetition time (TR) 5.68 ms, echo time (TE) 4.61 ms, slice thickness 5 mm, flip angle 10°. The field of view was 192 mm (aqueduct, C3) or 256 mm (L3), while the in-plane resolution was fixed to 0.75 x 0.75 $mm^2$. Two flow-encoded datasets were acquired with 11 radial spokes each yielding a temporal resolution of 125 ms per velocity map. The velocity encoding strength (VENC) was adapted according to the peak velocities of CSF or blood flow. While all measurements in the aqueduct and inside the spinal canal exploited low VENC values of 10 to 30 cm $s^{-1}$, measurements at C3 and L3 were repeated with a higher VENC of 60 to 100 cm $s^{-1}$ focussing on the large veins outside the spinal canal. Measurements in the aqueduct and at C3 were conducted with a 64-channel head coil, while measurements at L3 used suitable elements of an 18-channel thorax coil and a 32-channel spine coil.

# Data Analysis

Real-time flow MRI datasets were quantitatively analysed using CaFuR software (Fraunhofer Mevis, Bremen, Germany) [21] designed to accomplish automatic segmentation of flow signals in real-time image series. Manual definition of an initial ROI for the determination of through-plane flow was based on both signal intensities in magnitude images and corresponding phase difference values in velocity maps (see Fig. 1, right columns for representative examples). Further data processing was performed using Matlab (Mathworks, Massachusetts, USA).

To account for inadequate adherence to the visually instructed breathing protocol such as a delayed performance, affected data sets were shifted in time as described in previous studies [8].

Statistical analysis was performed using Python 3 to test for significant differences between normal and forced breathing in quantitative flow parameters and ROI sizes. To indicate altered flow dynamics regardless of its direction the magnitude of the flow was evaluated. Both, magnitude flow and ROI values, were averaged in time for the first and second part of the breathing protocol corresponding to unsigned-area-under-curve values for individual volunteers grouped into normal and forced breathing. To test for normal distribution (along volunteers) the Shapiro Wilk test was used and if applicable a paired t-test employed to calculate p-values. Alternatively, for non-normally distributed data, a Wilcoxon signed-rank test was applied and in both cases statistical significance accepted at p values $< 0.05$.

# Results

Figure 1 depicts original magnitude images and zoomed sections from real-time flow MRI acquisitions as well as corresponding velocity maps during forced inspiration and expiration, respectively. The examples cover the three slice positions at Aqd, C3, and L3 of three representative subjects. Rows a, b and d refer to CSF flow measurements within the cranium and spinal canal, while rows c and e illustrate the ROIs for cervical and abdominal venous flow.

Magnitude images possess a high sensitivity to through-plane flow because the inflow of previously unsaturated spins into the measurement section increases its signal intensity relative to the saturated spins within the slice. In velocity maps on the other hand, dark and bright signals correspond to opposite flow directions with grey values representing zero movement, i.e. stationary tissue. In all sections, the occurrence of bright signals in velocity maps refers to upward flow, while dark signals represent downward flow.

Flow dynamics of CSF and venous blood are depicted in Figs. 2 and 3. Figure 2 summarizes color-coded individual flow rates (ml $s^{-1}$) of the 12 subjects at each time point. No flow signal could be detected in the C3 EV for subject #6 and in L3 EV for subject #3. Mean-color coded flow rates averaged across subjects are shown in Fig. 3. The mean values across all subjects of the time-averaged magnitude flow (ml $s^{-1}$) are listed in Table 1.

Table 1
Mean magnitude flow during normal and forced breathing (mean ± SD across subjects).

| ROI | Mean Magnitude Flow (ml $s^{-1}$) | | |
|---|---|---|---|
| | normal | forced | p-value |
| Aqd | 0.02 ± 0.01 | 0.04 ± 0.03 | 0.001* |
| C3 CSF | 0.83 ± 0.36 | 1.08 ± 0.51 | 0.016* |
| C3 EV | 0.45 ± 0.49 | 0.49 ± 0.41 | 0.175 |
| C3 IJV | 6.8 ± 2.6 | 5.5 ± 2.2 | 0.0008* |
| L3 CSF | 0.15 ± 0.07 | 0.50 ± 0.38 | 0.004* |
| L3 EV | 0.19 ± 0.16 | 0.24 ± 0.17 | 0.175 |
| L3 IVC | 25.5 ± 7.5 | 28.7 ± 8.7 | 0.047* |

# Fluid dynamics during normal breathing

As a general observation, neither CSF nor venous blood flow reveal clear respiratory-driven dynamics during normal breathing. In the narrow aqueduct CSF flow was close to zero with magnitude values of 0.02 ± 0.01 ml $s^{-1}$ (Table 1). At C3 CSF flow is higher (0.83 ± 0.36 ml $s^{-1}$) and characterized by a cardiac-related pulsatility discernable in individual (Fig. 2) and mean flow rates (Fig. 3). CSF flow rates at L3 remain low (0.15 ± 0.07 ml $s^{-1}$).

Venous blood from the upper body reveals a continuous downward with a small cardiac-related component as depicted in Figs. 2 and 3 and Table 1. The mainly upward directed venous flow in the IVC (mean magnitude value 25.5 ± 7.5 ml $s^{-1}$) is characterized by modulations which follow individual pattern of normal free breathing (Fig. 2) and cancel when calculating mean values resulting in a relatively steady upward flow (Fig. 3). Flow in the EV (0.19 ± 0.16 ml $s^{-1}$) of the lumbar venous plexus exhibits considerable variability between subjects (Fig. 2).

During the final 10 s of the breathing protocol, i.e. after 40 s of forced breathing, flow dynamics of both fluid systems rapidly recover their pattern observable during initial rest as illustrated in Figs. 2 and 3.

# Fluid dynamics during forced breathing

Forced respiration during the 40–80 s period of the breathing protocol results in marked changes of CSF and venous flow dynamics. At all locations respiration induces high-amplitude flow modulations as illustrated for individual subjects (Fig. 2) and the mean flow rates (Fig. 3).

Forced inspiration elicits an increase of flow in cranial (upward) direction (coded in red) in the entire CSF system, i.e. at the aqueduct, C3 and L3, whereas forced expiration causes a caudal CSF movement

(coded in blue) though to a more variable extent. Mean magnitude flow was significantly higher in all CSF regions during forced breathing compared to free or normal breathing (Aqd: $p = 0.001$, C3: $p = 0.016$, L3: $p = 0.004$).

Flow in venous vessels EV and IJV at C3 immediately follows respiratory modulation yielding enhanced dynamics (Figs. 2 and 3). Mean magnitude flow tends to increase in EV ($p = 0.175$, Table 1), while IJV flow significantly decreases ($p = 0.0008$) over the course of 40 s forced breathing.

The flow dynamics in the veins of the lower body are also dominated by respiration, although with reversed directionality compared to the upper body. During deep inspiratory phases upward flow in the IVC at L3 abates or even reverses downward (coded in blue in Fig. 2) and rapidly returns during expiration leading to significantly increased mean magnitude flow values ($p = 0.047$, Table 1). A similar behavior is seen in the lumbar EV, yet with higher variability, e.g. compare subjects #1 and #5 in rows 1 and 5 of Fig. 2, L3 EV. The small mean magnitude flow values do not vary significantly ($p = 0.175$, Table 1) between the protocols.

# Frequency analysis of the flow signal during normal and forced breathing

Figure 4 depicts the frequency spectrum of flow dynamics in venous and CSF system during normal (left column) and forced breathing (right column), offering another perspective on cardiac (around 0.8–1.5 Hz) and respiratory related dynamics (< 0.5 Hz). During normal breathing, the maximum frequency components for CSF at Aqd and C3 are predominantly found in the range of heart rates (Aqd: 8/12 subjects, C3: 11/12) and even more distinctive for venous flow at C3 (12/12 in both ROIs). Conversely, at L3 the main frequencies for CSF as well as EV and IVC correspond to respiratory rates. During forced respiration the maximum frequency components are predominantly synchronized to 0.2 Hz which corresponds to the 5 s period of the breathing protocol. This holds true at all locations (Aqd: 11/12, C3: 7/12, IJV and EV: 10/11, L3 CSF and IVC: 11/12, L3 EV: 11/11).

# ROI sizes during normal and forced breathing

The temporal evolution of the individual ROI sizes ($mm^2$) for all 12 subjects is depicted in Suppl. Figure 1. In some subjects cardiac-related variations are discernable. ROI areas in C3 IJV and L3 IVC fluctuate in parallel to forced breathing. In 6 of the 7 ROIs, no consistent change over time during normal or forced respiration was observed and the comparison between both parts of the protocol revealed no significant changes (Suppl. Table 1). The ROI of the IJV at C3 showed a significant decrease in size ($p = 0.0023$) during 40 s of forced breathing which is in line with the reduction of flow at that position.

## Discussion

A central observation of this work is the fact that the dynamics of CSF and venous blood flow vary distinctly between normal and forced breathing thus corroborating the strong dependence on respiration.

While normal breathing has only very small measurable effects, the beginning of deep respiration causes immediate adherence of fluid dynamics to that driving force. In line with previous findings, forced inspiration elicits a distinct upward surge of CSF from the lumbar region up to the intracranial aqueduct. In contrast, forced expiration leads to reversed, downward flow albeit to a more varying extent. Venous outflow from the head/neck region is also modulated by forced respiration resulting in continuous inspiratory increases which so far has been demonstrated for the cervical epidural veins only [10, 22]. Simultaneously, the venous flow from the lower body up towards the heart abates at the onset of forced inspiration and rises quickly afterwards throughout expiration. In this study, flow in the lumbar EV could unequivocally be measured and its dynamics closely parallel that in the IVC (Fig. 3).

The rapid adjustments of CSF flow are considered to be prompted by the transmission of intrathoracic and intraabdominal pressure changes via abundant connections of the paravertebral venous plexus through the intervertebral foramina to the epidural spaces and their venous plexus therein [23, 24]. The amplified CSF movements during forced respiration resulted in a significant increase of time-averaged magnitude flow at all positions compared to free normal breathing for which low cardiac-related dynamics prevail (Table 1). As no significant variations in CSF ROI sizes occurred over time the rise of flow rates is ascribed to changes of flow velocity only (Suppl. Table 1).

The dominance of respiratory contributions to CSF velocities and flow volumes has been shown in several previous real-time flow MRI studies albeit mainly at the aqueduct and foramen magnum. For the aqueduct Takizawa et al. reported a greater amount of CSF displacement by respiratory than cardiac contributions, however, at lower velocities [25]. CSF velocity differences by a factor of two were found by Yildiz et al. between a cardiac and deep respiratory component at the foramen magnum, [26]. Furthermore, a recent computational study conducted by Vinje et al. demonstrated that small respiratory-induced pulsations of the ICP gradient induce CSF flow volumes dominating the cardiac component [27].

As demonstrated by the maximum frequency components of CSF flow, this study reveals a prompt transition from cardiac-related to respiration-dominated dynamics when moving from normal to forced breathing. Based on our results it seems plausible that the inspiratory decrease of the intrathoracic pressure has to surpass a certain threshold, i.e. the breath has to be deep enough, in order to facilitate any substantial fluid movement. The design of the current study did not include spirometry which may be used to quantify individual thresholds. However, we assume the values differ strongly among subjects depending on physiological parameters known to influence the individual breathing performance like height, age, gender as well as fitness level [28, 29]. Nevertheless, Figs. 2 and 3 suggest a common pattern of basic flow responses in all subjects regardless of the intersubject variability. The present findings therefore support the notion of interdependent CSF and venous dynamics, governed by intrathoracic and abdominal pressure changes and compensating each other in order to comply with the Monro-Kellie doctrines and to balance a constant intracranial volume.

In addition to IJV and cervical EV, real-time flow MRI measurements of venous flow comprised IVC and lumbar EV representing the lower body’s venous system. The constant venous drainage from the

head/neck region through IJV and EV alters distinctly with forced breathing and flow adheres to respiratory-driven patterns with amplification of outflow during every inspiration in agreement with previous studies [10, 30]. In concordance, the start of forced inspiration perturbs the steady venous return which prevails in the IVC during quiet breathing. Instantaneously, flow ceases and even briefly reverses downward. Forced breathing synchronized the venous flow dynamics yielding maximum frequency components in line with the breathing protocol. In particular, in the cervical region the frequency components completely abandoned the exclusive cardiac-related range.

The mean magnitude flow showed a trend towards higher numbers in cervical and lumbar EV and IVC reaching significance only in the latter ($p = 0.047$, Table 1). The effect was attributed largely to changes in velocity as variations in ROI sizes were not significant ($p = 0.26–0.588$, Suppl. Table 1). At the cervical level, we observed respiratory modulations in anterior and posterior cerebral venous outflow tracts [31]. While in the posterior EV flow tended to increase over 40 s forced breathing, mean magnitude flow values in the anterior IJV and consequently the ROI areas were found to decrease significantly. To our knowledge real-time cervical venous flow has not been studied during forced breathing in supine position so far. At this point, we can only speculate about the reasons for the discrepancy between outflow through the IJV and EV. Hypocapnia as a probable hyperventilatory effect might play a role. In this study we did not control $CO_2$ partial pressures, but explained signs of hyperventilation to the subjects and instructed them specifically to avoid these. Furthermore, hypocapnia affects cardiac output, arterial flow and to lesser extent cerebral blood volume [32–34]. Hence, its influence on the venous system might only be secondary and would be expected in all veins. Flow differences between these two cerebrovenous drainage pathways have so far been found in relation to postural changes. Multiple studies assigned the dominance of IJV drainage to the supine position and pointed to the EV systems as the major pathway in the upright position [35]. The bony spinal canal protects the thin valveless venous plexus from outer pressure changes and constant negative pleural and epidural pressures prevent the collapse of the vessels [13, 23, 35, 36]. In contrast, forced breathing might expose the IJV to various pressure changes along its course in the neck and at the entrance to the thoracic cavity.

The steep decrease and reversal of flow in the lower body IVC resulted in significantly increased magnitude flow values during forced breathing (Table 1) while ROI size remained vastly unchanged (Suppl. Table 1). A similar flow pattern has been reported by Joseph et al. applying real-time flow MRI [37]. Older studies based on clinical observations and invasive *in vivo* measurements of intracaval pressure and blood velocity also reported a paradoxical reduction of IVC flow parallel to deep inspiration [38, 39]. Here, simultaneous increase of abdominal pressure and reduction of intrathoracic pressure changed the IVC configuration from distended to collapsed at the level of the diaphragm as demonstrated by X-ray. The authors correlated the findings to a sharp anatomical constriction of the large vein where it passes though the diaphragm in postmortem casts and to the principles of flow through collapsible tubes [30, 38]. Small sizes and irregular anatomy usually impede *in vivo* flow MRI studies of lumbar EV. Hence, the results of 11/12 healthy subjects reported here represent one of the largest cohorts for flow measurements under physiological conditions. A trend towards higher magnitude flow values

was seen during forced breathing not reaching significance (p = 0.175, Table 1). Their dynamics parallel the behavior in the IVC with upward movements during expiration. In a recent study by Lloyd et al. flow in lumbar EV has been shown to preferentially move upward following respiratory modulations in line with our observations [40].

Spinal epidural space accommodates blood flow with opposite directionality. It is considered to form a discontinuous open compartment filled with fatty tissue and EV communicating with the thoracic and the abdominal cavity. Anatomical studies suggest morphological segmentations with traversing, interconnecting bundles of veins of varying density and configuration [41]. Interestingly, from the shape of the thoracic plexus segments and its flow characteristics during saline flushing, the authors hypothesized the presence of functional valves. Our results, which depict the opposite movements of venous blood towards the thoracic segment in response to respiration, may well align to that notion.

Over time numerous reports have postulated links between venous system pathologies and disorders of CSF circulation, comprising both superior and inferior caval systems. Compromised upper body venous flow plays a significant role in IIH, were increased intracranial pressure leads to headaches and papilledema, albeit the exact pathogenetic processes still remain unknown. Intracranial obstruction of venous outflow due to thrombosis, stenosis of e.g. transverse sinus or extracranial resistance due to obstructed IJV [42, 43] have been accounted for. Sleep-disordered breathing and subsequent cerebral venous hypertension are considered key factors in the development of symptomatic normal pressure hydrocephalus, prevalent among the elderly leading to ventriculomegaly and eventually dementia [44]. In infants, Shulman et al. related elevated pressure in the sagittal sinus to the occurrence of hydrocephalus [14].

Inferiorly, lumbar and sacral subarachnoid CSF spaces are affected by different epidural venous filling resulting from changes of blood volume or thoracic and abdominal pressures as illustrated in serial radiographs by Martins et al. [45]. Those rapid alteration of shapes of the CSF spaces after onset and end of venous system manipulations (e.g., by bilateral jugular compression) may serve as indication for the tight interplay between venous (epidural) and CSF fluid system.

The exact coupling mechanisms of cerebral blood flow and CSF movement are still investigated. The relationship between intracranial hemodynamics, brain tissue and CSF flow has been described by temporal waveform characteristics, their frequency compositions and application of transfer functions from blood to CSF flow [46, 47]. Recent studies disclosed a coherent correlation between neural slow waves, hemodynamic oscillations and CSF dynamics during non-rapid eye movement sleep [48]. In our awake subjects, we found that the venous and CSF system reacted simultaneous and complementary to each other if prompted by sufficient intrathoracic and abdominal pressure changes. Hence, it can be postulated that breathing and in particular forced respiration represents another physiological coupling mechanism for cranio-spinal fluid flow balance.

# Conclusions

In contrast to normal free breathing forced respiration leads to significant increases and prompt synchronization of flow dynamics in the CSF and venous systems. The lumbar caval and epidural venous upward surge during free breathing abates with the onset of forced inspiration and promptly rises during ensuing exhalation – a pattern opposite to that of venous flow in the upper body part. Spinal and intracranial CSF, on the other hand, move uniformly upwards during forced inhalation as previously described. It appears as if only surpassing a certain threshold of intrathoracic and abdominal volume and thus pressure changes can perturb the steady state of cardiac-dominated fluid dynamics prevailing during physical rest. Our results support the notion that deep respiration represents one coupling mechanism of interdependent venous and brain fluid flow. These insights into the tight interplay between CSF and venous fluid dynamics will also expand our understanding of the pathophysiology of human diseases with CSF flow disturbances such as hydrocephalus leading to new and more specific therapeutic options.

# Abbreviations

Aqd aqueduct
CSF cerebrospinal fluid
C3 cervical spine at level 3
EV epidural veins
IIH ideopathic intracranial hypertension
IJV internal jugular vein
IVC inferior vena cava
L3 lumbar spine at level 3
MRI magnetic resonance imaging
SD standard deviation
Th1 thoracic spine at level 1
Th8 thoracic spine at level 8

# Declarations

### Ethics approval and consent to participate

The study was approved by the institutional review board of the University Medicine Göttingen ((#18/2/14) and written informed consent was obtained from each subject prior to MRI. The study was in compliance with the Declaration of Helsinki.

### Consent for publication

not applicable

### Availability of data and material

The datasets used and/or analyzed during the current study are available from the corresponding author on reasonable request.

### Competing interests

The authors declare no competing financial interest.


### Funding

SDK, H-CL and JG gratefully acknowledge financial support by the Mrs. L. Grun funds.


### Authors' contributions

JK, LGR, and BE acquired and analyzed the MRI data. JK, LGR and SB analyzed, interpreted the data and contributed to the writing of the manuscript. H-CL designed the study and interpreted the data. JG interpreted the data and contributed to the writing of the manuscript. JF and SDK designed the study, interpreted the data and wrote the manuscript. All authors read and approved the final manuscript.


### Acknowledgements

We thank Prativa Sahoo, PhD and Hendrik Rosewich, MD for the support of the statistical analysis.


## References


1. Elvsashagen T, Mutsaerts HJ, Zak N, Norbom LB, Quraishi SH, Pedersen PO, et al. Cerebral blood flow changes after a day of wake, sleep, and sleep deprivation. Neuroimage. 2019;186:497-509.
2. Oreskovic D, Rados M, Klarica M. Role of choroid plexus in cerebrospinal fluid hydrodynamics. Neuroscience. 2017;354:69-87.
3. Xie L, Kang H, Xu Q, Chen MJ, Liao Y, Thiyagarajan M, et al. Sleep drives metabolite clearance from the adult brain. Science. 2013;342:373-7.
4. Jiang Q, Zhang L, Ding G, Davoodi-Bojd E, Li Q, Li L, et al. Impairment of the glymphatic system after diabetes. J Cereb Blood Flow Metab. 2017;37:1326-37.
5. Wardlaw JM, Benveniste H, Nedergaard M, Zlokovic BV, Mestre H, Lee H, et al. Perivascular spaces in the brain: anatomy, physiology and pathology. Nat Rev Neurol. 2020;16:137-53.
6. Bock HC, Dreha-Kulaczewski SF, Alaid A, Gartner J, Ludwig HC. Upward movement of cerebrospinal fluid in obstructive hydrocephalus-revision of an old concept. Childs Nerv Syst. 2019;35:833-41.
7. Frahm J, Voit D, Uecker M. Real-Time Magnetic Resonance Imaging: Radial Gradient-Echo Sequences With Nonlinear Inverse Reconstruction. Invest Radiol. 2019;54:757-66.
8. Aktas G, Kollmeier JM, Joseph AA, Merboldt KD, Ludwig HC, Gartner J, et al. Spinal CSF flow in response to forced thoracic and abdominal respiration. Fluids Barriers CNS. 2019;16:10.

9. Dreha-Kulaczewski S, Joseph AA, Merboldt KD, Ludwig HC, Gartner J, Frahm J. Inspiration is the major regulator of human CSF flow. J Neurosci. 2015;35:2485-91.
10. Dreha-Kulaczewski S, Joseph AA, Merboldt KD, Ludwig HC, Gartner J, Frahm J. Identification of the Upward Movement of Human CSF In Vivo and its Relation to the Brain Venous System. J Neurosci. 2017;37:2395-402.
11. Greitz D, Wirestam R, Franck A, Nordell B, Thomsen C, Stahlberg F. Pulsatile brain movement and associated hydrodynamics studied by magnetic resonance phase imaging. The Monro-Kellie doctrine revisited. Neuroradiology. 1992;34:370-80.
12. Nakada T, Kwee IL. Fluid Dynamics Inside the Brain Barrier: Current Concept of Interstitial Flow, Glymphatic Flow, and Cerebrospinal Fluid Circulation in the Brain. Neuroscientist. 2019;25:155-66.
13. Ludwig HC, Bock H, Gärtner J, Schiller S, Frahm J, Dreha-Kulaczewski S. Hydrocephalus revisited: New insights into dynamics of neurofluids on macro- and microscales. Preprints 2020120322 2020.
14. Shulman K, Ransohoff J. Sagittal sinus venous pressure in hydrocephalus. J Neurosurg. 1965;23:169-73.
15. Haacke EM, Beggs CB, Habib C. The role of venous abnormalities in neurological disease. Rev Recent Clin Trials. 2012;7:100-16.
16. Morris PP, Black DF, Port J, Campeau N. Transverse Sinus Stenosis Is the Most Sensitive MR Imaging Correlate of Idiopathic Intracranial Hypertension. AJNR Am J Neuroradiol. 2017;38:471-7.
17. Joseph AA, Merboldt KD, Voit D, Zhang S, Uecker M, Lotz J, et al. Real-time phase-contrast MRI of cardiovascular blood flow using undersampled radial fast low-angle shot and nonlinear inverse reconstruction. NMR Biomed. 2012;25:917-24.
18. Unterberger MJ, Holzapfel GA. Advances in the mechanical modeling of filamentous actin and its cross-linked networks on multiple scales. Biomech Model Mechanobiol. 2014;13:1155-74.
19. Bernstein MA, Zhou XJ, Polzin JA, King KF, Ganin A, Pelc NJ, et al. Concomitant gradient terms in phase contrast MR: analysis and correction. Magn Reson Med. 1998;39:300-8.
20. Tan Z, Roeloffs V, Voit D, Joseph AA, Untenberger M, Merboldt KD, et al. Model-based reconstruction for real-time phase-contrast flow MRI: Improved spatiotemporal accuracy. Magn Reson Med. 2017;77:1082-93.
21. Chitiboi T, Hennemuth A, Tautz L, Huellebrand M, Frahm J, Linsen L, et al. Context-based segmemtation and analysis of multi-cycle real-time cardiac MRI. IEEE International Symposium on Biomedical Imaging. 2014:943-6.
22. Dreha-Kulaczewski S, Konopka M, Joseph AA, Kollmeier J, Merboldt KD, Ludwig HC, et al. Respiration and the watershed of spinal CSF flow in humans. Sci Rep. 2018;8:5594.
23. Henriques CQ. The veins of the vertebral column and their role in the spread of cancer. Ann R Coll Surg Engl. 1962;31:1-22.
24. Stringer MD, Restieaux M, Fisher AL, Crosado B. The vertebral venous plexuses: the internal veins are muscular and external veins have valves. Clin Anat. 2012;25:609-18.

25. Takizawa K, Matsumae M, Sunohara S, Yatsushiro S, Kuroda K. Characterization of cardiac- and respiratory-driven cerebrospinal fluid motion based on asynchronous phase-contrast magnetic resonance imaging in volunteers. Fluids Barriers CNS. 2017;14:25.
26. Yildiz S, Thyagaraj S, Jin N, Zhong X, Heidari Pahlavian S, Martin BA, et al. Quantifying the influence of respiration and cardiac pulsations on cerebrospinal fluid dynamics using real-time phase-contrast MRI. J Magn Reson Imaging. 2017;46:431-9.
27. Vinje V, Ringstad G, Lindstrom EK, Valnes LM, Rognes ME, Eide PK, et al. Respiratory influence on cerebrospinal fluid flow - a computational study based on long-term intracranial pressure measurements. Sci Rep. 2019;9:9732.
28. Kaneko H, Horie J. Breathing movements of the chest and abdominal wall in healthy subjects. Respir Care. 2012;57:1442-51.
29. Konno K, Mead J. Measurement of the separate volume changes of rib cage and abdomen during breathing. J Appl Physiol. 1967;22:407-22.
30. Wexler L, Bergel DH, Gabe IT, Makin GS, Mills CJ. Velocity of blood flow in normal human venae cavae. Circ Res. 1968;23:349-59.
31. Epstein HM, Linde HW, Crampton AR, Ciric IS, Eckenhoff JE. The vertebral venous plexus as a major cerebral venous outflow tract. Anesthesiology. 1970;32:332-7.
32. Laffey JG, Kavanagh BP. Hypocapnia. N Engl J Med. 2002;347:43-53.
33. Zhang Z, Guo Q, Wang E. Hyperventilation in neurological patients: from physiology to outcome evidence. Curr Opin Anaesthesiol. 2019;32:568-73.
34. Tercero J, Gracia I, Hurtado P, de Riva N, Carrero E, Garcia-Orellana M, et al. Effects on cerebral blood flow of position changes, hyperoxia, CO2 partial pressure variations and the Valsalva manoeuvre: A study in healthy volunteers. Eur J Anaesthesiol. 2021;38:49-57.
35. Valdueza JM, von Munster T, Hoffman O, Schreiber S, Einhaupl KM. Postural dependency of the cerebral venous outflow. Lancet. 2000;355:200-1.
36. Groen RJ, Grobbelaar M, Muller CJ, van Solinge G, Verhoof O, du Toit DF, et al. Morphology of the human internal vertebral venous plexus: a cadaver study after latex injection in the 21-25-week fetus. Clin Anat. 2005;18:397-403.
37. Joseph AA, Voit D, Frahm J. Inferior vena cava revisited - Real-time flow MRI of respiratory maneuvers. NMR Biomed. 2020;33:e4232.
38. Gardner AM, Turner MJ, Wilmshurst CC, Griffiths DJ. Hydrodynamics of blood flow through the inferior vena cava. Med Biol Eng Comput. 1977;15:248-53.
39. Usubiaga JE, Moya F, Usubiaga LE. Effect of thoracic and abdominal pressure changes on the epidural space pressure. Br J Anaesth. 1967;39:612-8.
40. Lloyd RA, Butler JE, Gandevia SC, Ball IK, Toson B, Stoodley MA, et al. Respiratory cerebrospinal fluid flow is driven by the thoracic and lumbar spinal pressures. J Physiol. 2020;598:5789-805.

41. Groen RJ, Groenewegen HJ, van Alphen HA, Hoogland PV. Morphology of the human internal vertebral venous plexus: a cadaver study after intravenous Araldite CY 221 injection. Anat Rec. 1997;249:285-94.
42. Ball AK, Clarke CE. Idiopathic intracranial hypertension. Lancet Neurol. 2006;5:433-42.
43. Wilson MH. Monro-Kellie 2.0: The dynamic vascular and venous pathophysiological components of intracranial pressure. J Cereb Blood Flow Metab. 2016;36:1338-50.
44. Roman GC, Jackson RE, Fung SH, Zhang YJ, Verma AK. Sleep-Disordered Breathing and Idiopathic Normal-Pressure Hydrocephalus: Recent Pathophysiological Advances. Curr Neurol Neurosci Rep. 2019;19:39.
45. Martins AN, Wiley JK, Myers PW. Dynamics of the cerebrospinal fluid and the spinal dura mater. J Neurol Neurosurg Psychiatry. 1972;35:468-73.
46. Baledent O, Gondry-Jouet C, Meyer ME, De Marco G, Le Gars D, Henry-Feugeas MC, et al. Relationship between cerebrospinal fluid and blood dynamics in healthy volunteers and patients with communicating hydrocephalus. Invest Radiol. 2004;39:45-55.
47. Schmid Daners M, Knobloch V, Soellinger M, Boesiger P, Seifert B, Guzzella L, et al. Age-specific characteristics and coupling of cerebral arterial inflow and cerebrospinal fluid dynamics. PLoS One. 2012;7:e37502.
48. Fultz NE, Bonmassar G, Setsompop K, Stickgold RA, Rosen BR, Polimeni JR, et al. Coupled electrophysiological, hemodynamic, and cerebrospinal fluid oscillations in human sleep. Science. 2019;366:628-31.

# Figures

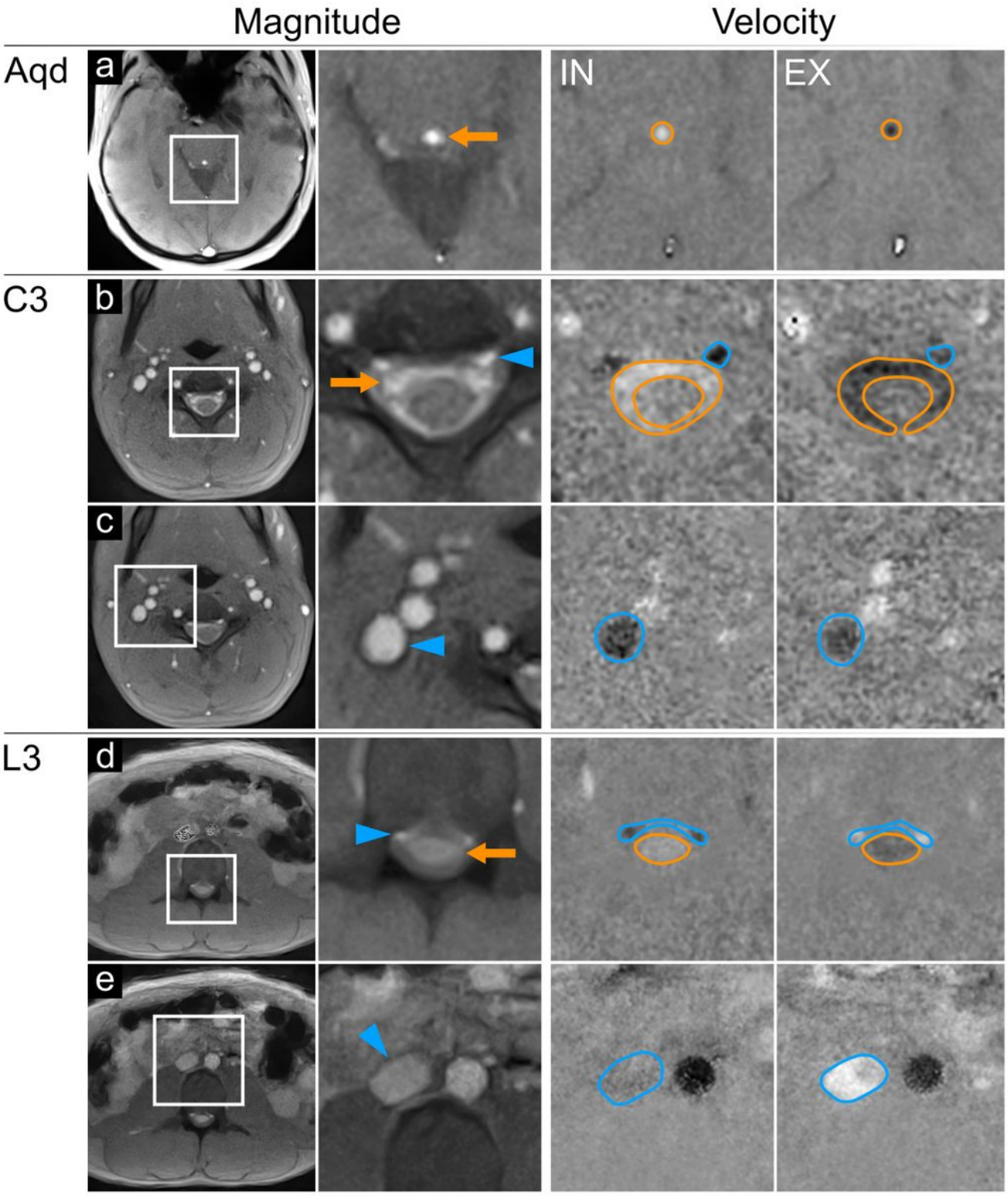


**Figure 1**

Regions of interest for CSF and venous flow analyses. Magnitude images (left columns) in normal and magnified views at the aqueduct. Aqd (a; subject #2), spinal cervical level C3 (b, c; subject #10), and lumbar level L3 (d, e; subject #5). CSF flow (orange arrows) appears as bright signal in the Aqd (a), the subarachnoid spaces at C3 (b) and L3 (d). Flow in cervical (b) and lumbar (d) epidural veins (blue arrow heads) and in IJV (c) and IVC (e). Velocity maps (right columns) during forced inspiration IN and

expiration EX. Magnified maps indicate upward CSF flow (bright signals in orange ROIs) at all levels (a, b, d) during IN. Spinal epidural veins (b, d) and IJV (c) show simultaneous downward flow (dark signal in blue ROIs). Of note, flow in IVC (blue ROI, e) subsides (grey signal). Downward CSF flow (dark signal) occurred at all levels (a, b, d) during EX. Flow in epidural veins at C3 appears less dark (b), hence alleviated. Lumbar epidural veins (d) and ICV (e) show upward blood flow (bright). Aqd = aqueduct; C3 = cervical level 3; L3 = lumbar level 3; EV = epidural veins; IJV = internal jugular vein; IVC = inferior vena cava.

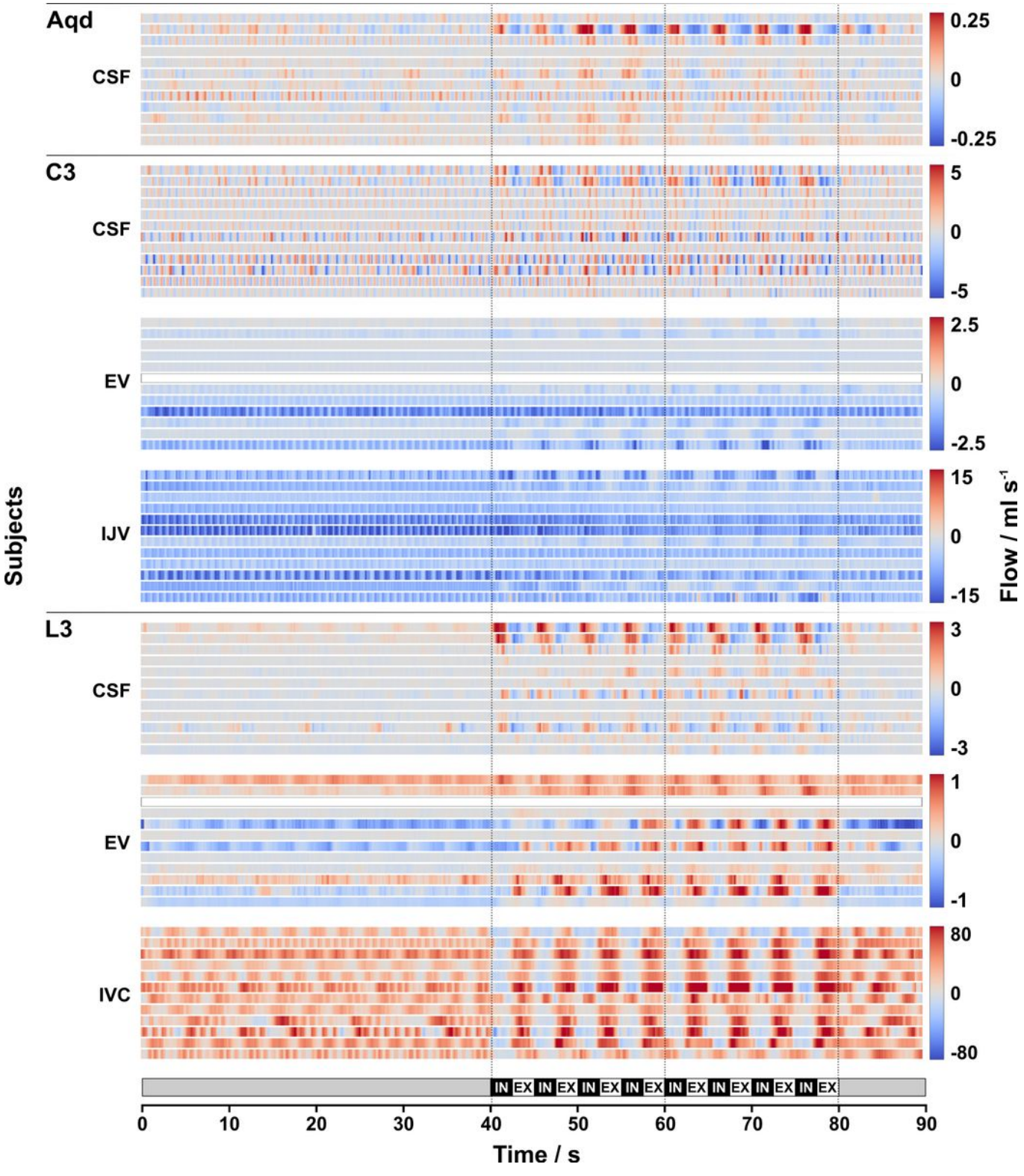

## Figure 2

Individual CSF and venous flow. Color-coded flow rates (ml s-1) of all 12 subjects in 12 horizontal lines for each ROI during 90 s breathing protocol (bottom). Vertical lines mark start, middle and end of forced breathing. Note the different scaling for the various ROIs. Normal breathing (0-40 s): low CSF flow (blue = downward; red = upward) is regulated by cardiac pulsation (e.g., in Aqd and L3). Venous blood shows steady downward flow in EV and IJV with cardiac pulsatility. ICV flow is predominantly in upward direction with cardiac and respiratory influences (e.g., #1, #4, #5). Low flow at L3 EV is variable between subjects (opposite directionality e.g., #10, #5). Forced breathing (40-80 s): CSF and venous flow synchronized to respiration. During IN CSF moves upwards in all ROIs (red), downward venous flow in C3 EV and IJV becomes further enhanced (darker blue). Upward flow in IVC and L3 EV ceases or reverses (blue). During EX downward CSF movement (blue) prevails at all locations, venous flow decreases (lighter blue) at C3 and resumes upward directionality at L3 (red). L3 EV flow in subjects #1 and #2 show opposite behavior. Normal breathing (80-90 s): rapid return of CSF and blood flow to the initial pattern. Aqd = aqueduct; C3 = cervical level 3; L3 = lumbar level 3; EV = epidural veins; IJV = internal jugular vein; IVC = inferior vena cava; IN = inspiration, EX = expiration.

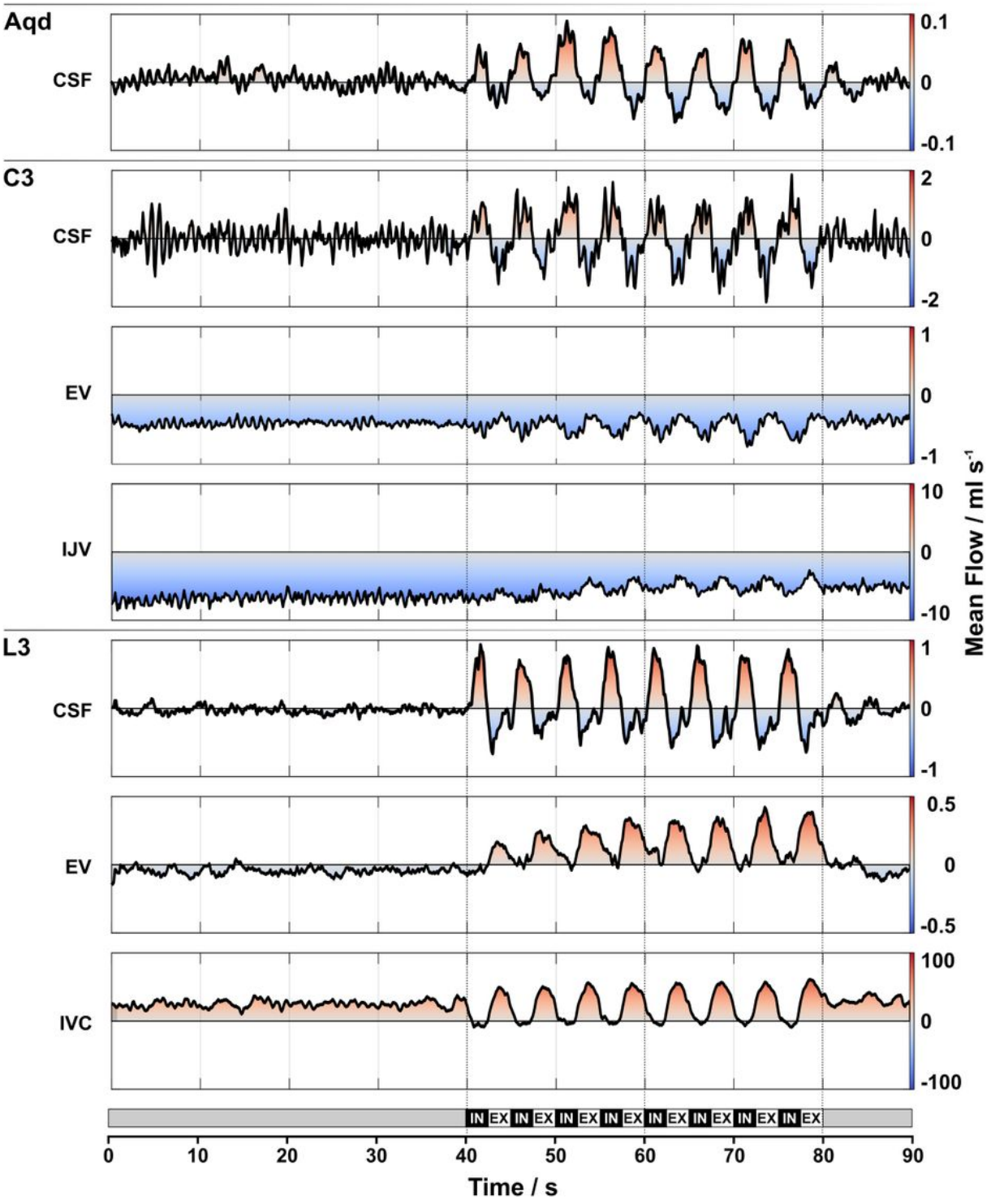


## Figure 3

Mean CSF and venous flow. Color-coded mean flow rates (ml s-1) of CSF and venous blood averaged across subjects at all locations during the 90 s breathing protocol (bottom). Note the different scaling for the various ROIs. Normal breathing (0-40 s): low CSF flow with cardiac pulsatility. Venous flow in C3 EV and IJV remains constantly negative (blue). ICV shows upward (red) and L3 EV downward flow (light blue). Forced breathing (40-80 s): synchronous increase of CSF and venous flow following respiration.

CSF moves upwards with IN in all ROIs (red) and downwards during EX (blue). Venous blood shows downward flow at C3 and upward flow at L3. Normal breathing (80-90 s): rapid return of CSF and blood flow to the initial pattern. Aqd = aqueduct; C3 = cervical level 3; L3 = lumbar level 3; EV = epidural veins; IJV = internal jugular vein; IVC = inferior vena cava; IN = inspiration, EX = expiration.

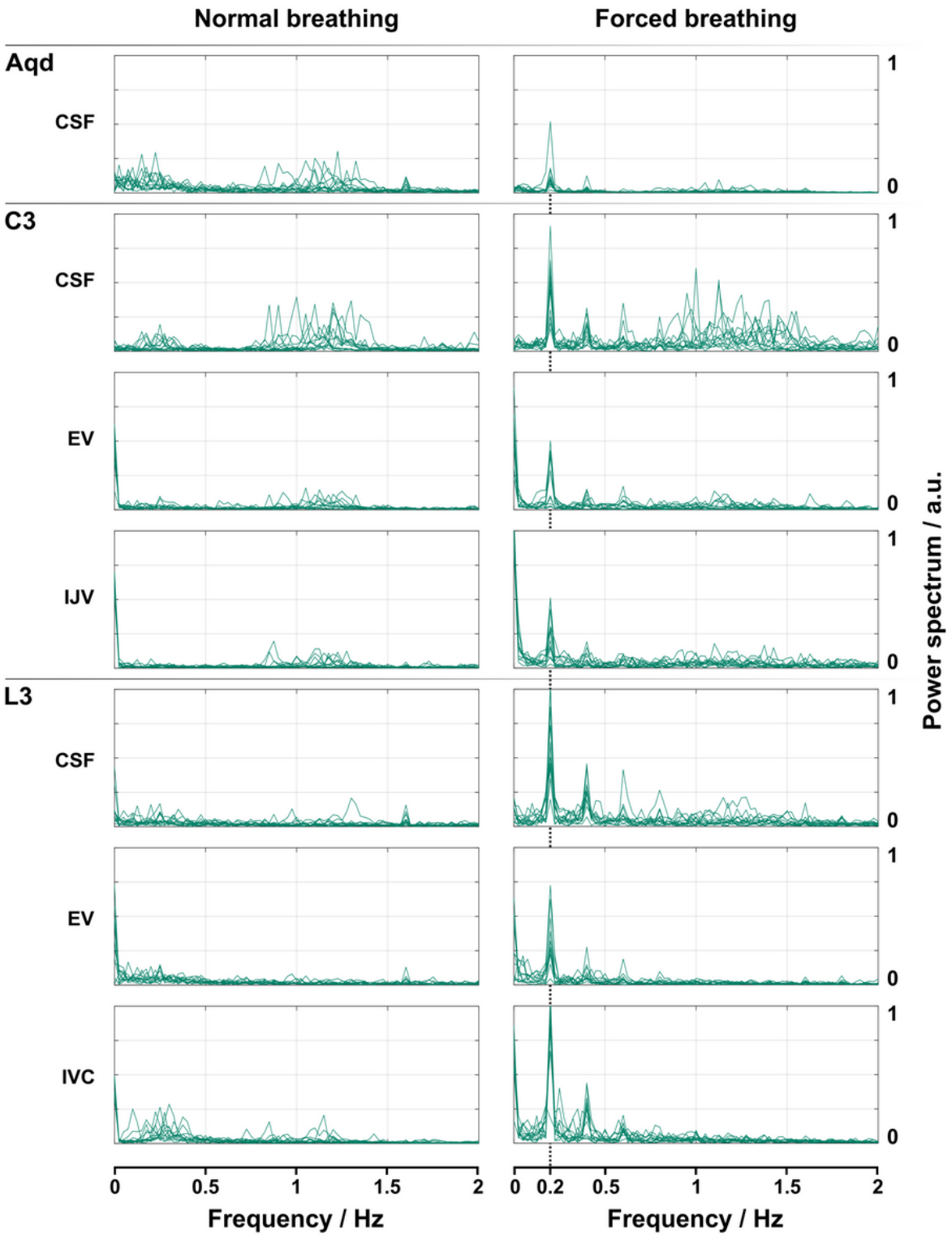


Figure 4

Spectral analysis of CSF and venous flow. Frequencies (Hz) of flow signals of all 12 subjects during normal (left) and forced breathing (right). Note the predominance of frequencies corresponding to heart rates during normal breathing for CSF (Aqd, C3) and C3 venous flow. At L3 frequencies related to quiet respiration prevailed. During forced breathing frequencies of 0.2 Hz (5 s = one breathing cycle in the protocol) and 0.4 Hz (2.5 s = half a breathing cycle) dominated at all locations in both fluid systems. Only at C3 CSF maximum frequency components corresponded to heart rates in 5 subjects (#4, 8, 9, 11, 12). Aqd = aqueduct; C3 = cervical level 3; L3 = lumbar level 3; EV = epidural veins; IJV = internal jugular vein; IVC = inferior vena cava.

## Supplementary Files

This is a list of supplementary files associated with this preprint. Click to download.

- SupplFig1ROISizescouplingCSFvenousfluidKollmeier.jpg
- SupplTable1ROIareasKollmeier.docx